Prediction of inter-particle capillary forces for non-perfectly wettable granular assemblies

Harireche, Ouahid; Faramarzi, Asaad; Alani, Amir M.

DOI:
10.1007/s10035-015-0581-1

Document Version
Peer reviewed version

Citation for published version (Harvard):
Harireche, O, Faramarzi, A & Alani, AM 2015, 'Prediction of inter-particle capillary forces for non-perfectly wettable granular assemblies', Granular Matter, vol. 17, no. 5, pp. 537-543. https://doi.org/10.1007/s10035-015-0581-1

Prediction of inter-particle capillary forces for non-perfectly wettable granular assemblies

Ouahid Harireche (Email: O.Harireche@gre.ac.uk)
Department of Civil Engineering, Faculty of Engineering & Science, University of Greenwich, Central Avenue, Chatham Maritime, Kent, ME4 4TB, United Kingdom

Asaad Faramarzi (Corresponding Author, Email: A.Faramarzi@bham.ac.uk)
School of Civil Engineering, University of Birmingham, Edgbaston, Birmingham B15 2TT, United Kingdom

Amir M. Alani (Amir.Alani@uwl.ac.ul)
School of Computing and Technology, University of West London, London W5 2PA, United Kingdom

Abstract

At a moisture content that corresponds to the so-called pendular regime, granular assemblies are subjected to the development of inter-particle capillary forces. These forces provide a tensile resistance at the particle level, which results into a cohesion shear strength at the macroscopic scale. Granular assemblies with non-perfectly wettable particles show a non-zero contact angle between the liquid bridge and the particle surface. It is worth mentioning that such an angle is an intrinsic property of the particle pair in contact and the liquid bridge. Its value has a significant effect on the magnitude of the capillary force and its behaviour as a function of the particle separation distance. This study is mainly motivated by the large range of values of the contact angle observed experimentally. In this paper, the governing equations for non-perfectly wettable granular assemblies in the pendular regime are first developed using the toroidal approximation. A robust numerical procedure is then proposed to solve these equations. Experimental validation of the numerical model shows that the capillary forces are predicted with a very good accuracy. The influence of the contact angle on the predicted inter-particle capillary force is also discussed.

Keywords

Granular assemblies; Capillary forces; Non-perfectly wettable particles ; Toroidal approximation

1 Introduction

Since the fundamental theories on capillary cohesion developed by Haines [1, 2] and Fisher [3, 4] and further developments by later scholars such as Carman [5], Rose [6] and Mason and Clark [7], investigations on the magnitude and stability of capillary forces are still of interest in various fields. To date, the particular case of equal size particles has received much more attention, especially in various attempts to develop theoretical predictions of capillary forces. For instance, the study by Lian et al. [8] was limited to this particular context, although stability and non-perfectly wettable particles have been taken into consideration. A work undertaken by Willet et al. [9] provided an interesting experimental basis for validation, although no control of the contact angle was performed in these experiments, which were conducted with remarkable care to maintain perfect surface condition of the tested particles. Willet et al. [9] performed numerical predictions of capillary forces for equal sized particles. They also extended their approach to unequal size particles using Derjaguin approximation. Schwarze et al. [10] implemented a simple liquid bridge model, based on Willet et al. [9] approximate model, into a software package based on discrete element method (DEM) in order to simulate shear cell experiments. More recently, Harireche et al. [11] proposed a toroidal approximation of capillary forces for polydisperse granular assemblies. Their model was successfully validated for a wide range of particle polydispersity against the experimental data obtained by Willet et al. [9]. However, the framework they proposed was limited to perfectly wettable particles. In the present work, the toroidal model proposed by Harireche et al. [11] is extended to non-perfectly wettable granular assemblies. This study is particularly motivated by the wide range of values of the contact angle observed experimentally. In the present paper, the toroidal model is first presented in the general context of non-perfectly wettable particles. Governing equations are developed within the frame of a normalised geometry and are valid for any particle-pair and liquid bridge configuration. A robust numerical procedure is then proposed to solve the resulting non-linear system, which consists of five equations. The five unknowns characterise the particle pair and liquid bridge geometry and the equations must be solved for given values of the contact angle, liquid volume and particles' separation distance.

2 A toroidal model for non-perfectly wettable particles

2.1 Normalised geometry of particle-pair and liquid bridge

The toroidal approximation of the liquid bridge assumes the meridian profile of the liquid-air interface to have a circular shape. In the present study, the contact angle θ is considered as an intrinsic property of the particle pair and liquid bridge and is assumed to be independent of the separation distance d (Fig. 1). The particle-pair consists of two grains P_A and P_B of spherical shape with radii R_A and R_B ($R_A \geq R_B$).

In order to obtain relations that are independent of the geometry and configuration of the particle pair, all length measures are normalised with respect to the radius R_A of the largest particle and we denote r the ratio of particle radii.

$$r = \frac{R_B}{R_A} \tag{1}$$

The normalised geometry of a non-perfectly wettable ($\theta \neq 0$) particle-pair and liquid bridge is illustrated in Figure 1. In this normalised geometry, the half-filling angles are denoted ψ and χ respectively and d is the inter-particle separation distance. The circular arc representing the profile of the liquid bridge has a centre Ω with coordinates ξ and η in the rectangular system of coordinates with origin at the centre A of particle P_A. The circle used to model the meridian profile of the liquid bridge crosses the two particles. The tangents to the liquid surface and to the particle surface at the intersection point make an angle, which is referred to as the contact angle and is denoted as θ. According to the Toroidal approximation, the external radius of curvature ρ of the liquid bridge is constant. The internal radius of curvature has a minimum value, $\rho_i = \eta - \rho$ at the bridge neck.

Denoting V_w the liquid volume in the liquid bridge, the non-dimensional expression of this volume is

$$V_w^* = \frac{V_w}{\left(R_A\right)^3} \tag{2}$$

Harireche et al. [11] derived two limit configurations which present lower and upper bounds to the normalised liquid volume. These two limit configurations define a maximum value, ρ_{max} and a minimum value, ρ_{min} for the external radius of curvature. These values are only valid for the perfectly wettable case but, as will be seen later, they are important to the solution procedure of the general problem. Expressions of these maximum and minimum radii of curvature ρ_{max} and ρ_{min} have been obtained in Harireche et al. [11].

2.2 Normalised capillary force

Fisher [3] derived an expression where the capillary force *F* is the sum of two forces due to surface tension σ and matric suction s_u. In the present model, the capillary force is obtained at the bridge neck where the scaled internal radius of curvature is ρ_i.

$$F_c = 2\pi\left(R_A\rho_i\right)\sigma + \pi\left(R_A\rho_i\right)^2 s_u \tag{3}$$

The method adopted here evaluates the solution at the bridge neck and is referred to as the"gorge" method. This method has been proven to provide the most accurate estimate of the capillary force, compared to the evaluation of this force at the three-phase contact line, for example. This conclusion has been verified by Lian et al., [8].

The matric suction is expressed in terms of surface tension and curvature radii of the liquid bridge, according to the so-called *Laplace-Young equation* below:

$$s_u = \sigma\left(\frac{1}{R_A\rho} - \frac{1}{R_A\rho_i}\right) \tag{4}$$

The normalised capillary force is denoted F_c^* and its magnitude at the bridge neck is defined by combining equations (3) and (4).

$$F_c^* = \frac{\eta}{\rho}\left(\eta - \rho\right) \tag{5}$$

The capillary force at the bridge neck is given by

$$F_c = \pi R_A \sigma F_c^* \tag{6}$$

2.3 Fundamental equations governing particle pair, liquid bridge and capillary force

In the general context of non-perfectly wettable particle-pair (Fig. 1) the liquid bridge geometry and hence, the magnitude of the capillary force, is affected by the five parameters: ρ , ξ , η , ψ , χ . For a given normalised liquid volume, a normalised separation distance and a contact angle, these parameters are uniquely determined by the following five conditions:

$$y(x_A) = \sin\psi\,; \qquad x_A = \cos\psi \tag{7}$$

$$y(x_B) = r\sin\chi\,; \qquad x_B = L - r\cos\chi \tag{8}$$

where $L \equiv 1 + d + r$ is the normalised distance between particles' centres.

$$y'(x_A) = -\tan\delta_A; \qquad \delta_A = \frac{\pi}{2} - (\theta + \psi) \tag{9}$$

$$y'(x_B) = \tan\delta_B\,; \qquad \delta_B = \frac{\pi}{2} - (\theta + \chi) \tag{10}$$

$$\left(\int_{\cos\psi}^{L - r\cos\chi} \pi y^2 dx\right) - V_A^* - V_B^* = V_w^* \tag{11}$$

where V_A^* and V_B^* are the volumes of the spherical caps on particle P_A and particle P_B respectively (Fig. 2).

$$V_I^* = \frac{\pi h_I}{6}\left(3y_I^2 + h_I^2\right);\ \ I = A, B \tag{12}$$

$$y_A \equiv y(x_A)\,,\ y_B \equiv y(x_B)\,,\ h_A = 1 - \cos\psi\,,\ h_B = r(1 - \cos\chi) \tag{13}$$

Conditions (7) and (8) correspond to the expressions of the coordinates of points A and B where the extended arc representing the liquid bridge profile crosses the two particles' circular contours (Fig. 1). Conditions (9) and (10) correspond to the required contact angle θ at points A and B. Condition (11) corresponds to the required normalised liquid volume. Note that all these conditions are expressed in the normalised geometry.

After evaluating the integral term in equation 11, this equation can be rewritten under the form:

$$\pi\left(F_v(x_B) - F_v(x_A)\right) - V_A^* - V_B^* = V_w^* \tag{14}$$

Where

$$F_v(x) = -\frac{1}{3}(x-\xi)^3 + (x-\xi)(\eta^2+\rho^2) - \eta(x-\xi)(\eta-y) + \eta\rho^2 \arctan\left[-\frac{x-\xi}{\eta-y}\right] \quad (15)$$

If not impossible, an analytical solution to the non-linear system of equations 7-10 and 14 would be very difficult to obtain. Such a solution has not been attempted in the present work; we rather propose the numerical procedure described in the next section.

3 Numerical procedure for the calculation of the capillary force

For a given configuration of the particle-pair, defined by the parameters r and d and a contact angle θ, the present numerical approach provides an approximation of the capillary force, F_c developed by a liquid bridge of normalised liquid volume V_w^*.

Equations 7-10 and 14 can be cast under the form:

$$f_a(\boldsymbol{X}) = 0\,,\ a = 1,\ldots,5 \quad (16)$$

Where

$$\boldsymbol{X}^T = (x_A, x_B, \xi, \eta, \rho) \quad (17)$$

Note that for convenience, we use x_A and x_B as primary unknowns instead of the half-filling angles ψ and χ. Functions f_i can be easily identified. For completeness, these functions are provided in appendix 1. The Jacobian matrix of system (16) is defined by

$$J_{ab} = \frac{\partial f_a}{\partial X_b} \quad (18)$$

and is provided in appendix 2.

For a given contact angle θ, the interval $[0,\theta]$ is divided into *N-1* increments $[\theta_n, \theta_{n+1}]$, $n = 1,\ldots,N-1$ such that $\theta_1 = 0$ and the contact angle increment, $\Delta\theta = \theta_{n+1} - \theta_n$ is constant. At the first increment, the calculation process starts with a trial solution $\boldsymbol{X}^{(1)}$ that corresponds to $\theta_1 = 0$. Such a solution can be obtained using the secant procedure proposed by Harireche et al. [11]. It is important to note that for this first step where the contact angle is zero, the liquid bridge profile corresponds to the perfectly wettable

case. In this particular case the circle representing the liquid bridge in the normalised geometry is tangent to the particle pair. Such a circle is uniquely determined by the radius, which can be used as the primary unknown in this particular case.

The solution $\boldsymbol{X}^{(2)}$ at $\theta_2 = \theta_1 + \Delta\theta$ is then calculated using a Newton-Raphson iterative process starting from $\boldsymbol{X}^{(1)}$ as an initial guess. Once convergence is achieved, iterations for the next contact angle increment start with $\boldsymbol{X}^{(2)}$ as the initial guess. The algorithm provided in appendix 3 outlines the main steps in the calculation procedure.

4 Validations and discussion

Predictions based on the theoretical procedure presented in previous sections have been compared to the experimental data provided by Rabinovich et al. [12]. In these experiments, capillary forces were measured between glass spheres 38 -70 μm in diameter (Fig. 3). White mineral oil of "sharpening stone" grade was used to form the liquid bridge between the two spheres. In all experiments the smaller sphere has a radius of 19 μm and the contact angle is 10^{o}. The liquid surface tension is 27.5 mN/m. In experiments 1, 2 and 3 the radius of the larger sphere has values 35 μm, 32.5 μm and 27.5 μm, respectively. The liquid volume has values 2×10^{8} nm^3, 12×10^{8} nm^3 and 36×10^{8} nm^3, respectively. Figure 3 shows a very good agreement between the measured capillary forces and those predicted by the model developed in this study. As mentioned by Rabinovich et al. [12], there are maxima in the magnitude of the capillary force present at small separation distances (less than 10 nm), which are not clearly seen on the experimental data reproduced in Figure 3 because of the large scale of the abscissa. According to these authors, these maxima are believed to be due to contact angle hysteresis. The same phenomenon has been reported by Willet et al. [13].For comparison predictions by the proposed analytical expressions in Rabinovich et al. [12] are also depicted in Figure 3 (dashed lines). It is evident that this expression has overestimated the capillary force in all three cases and the proposed model in this study is in a better agreement with the experimental data particularly for curves (1) and (2).

It should be noted that Rabinovich et al. [12] have used "fitting values" for surface tension within the range 24-28 mN/m instead of the constant value of 27.5 mN/m. This fitting range corresponds to a percentage error of 10%. In the present work, for a fair comparison, a constant value of surface tension of 27.5 mN/m is used to calculate

capillary forces in both models for the three experiments (Fig. 3). Furthermore, since the analytical expression proposed by Rabinovich et al. [12] does not take into account for polydisperse assemblies, an effective particle radius is used in the calculations.

5 Parametric study of the developed model

In order to investigate the effect of the contact angle on the inter-particle capillary force, we carry out a set of qualitative simulations using the model developed in this study. To this effect, the combining effects of the contact angle with separation distance, liquid volume, and the ratio of particle radii, on the capillary force are considered.

5.1 Effect of contact angle and separation distance on capillary force

A particle pair with radii 2.381 and 1.588 mm (r = 0.667) and an inter-particle liquid with a surface tension of $\sigma = 2.06 \times 10^{-5}$ N/mm and a volume of $V_w = 1.32 \times 10^{-2}$ mm^3 is considered. The effect of contact angle on the inter-particle capillary force is shown in Figure 4. The figure shows that by increasing the contact angle, the capillary force is reduced; a similar trend to those reported in Willet et al. [9]. It is interesting to note that such effect is much more pronounced at small separation distances and is significantly reduced as the capillary bridge rupture distance is approached.

5.2 Effect of contact angle and liquid volume on capillary force

In this section we consider same particle pair as in section 5.1 above. The inter-particle liquid is also assumed to have same properties as in section 5.1. Two different contact angles (0 and 40 degrees) and two different scaled liquid volumes (V^*_w = 0.0001 and V^*_w = 0.001), making a total of four simulation scenarios, are considered. Figure 5 shows the results of these simulations. It is clear from this figure that while the initial capillary force is governed by the contact angle, the rate at which the inter-particle force decreases for an increasing separation distance depends on the liquid volume. In all cases the cubic root of the liquid volume provides a very good approximation of the rupture distance regardless of the contact angle values.

5.3 Effect of contact angle and ratio of particle radii on capillary force

Figure 6 shows the model predictions for three different ratios of particle radii, each at two different contact angles. This figure shows that, regardless of the contact angle, the capillary force increases as the ratio of particle radii increases. The difference in capillary force for different ratios of particle radii fades away as the separation distance increases. However there is a clear difference between force-separation curves corresponding to contact angles of 0° and 40°. This shows the importance and influence of contact angle on the capillary force. For instance, at a very small separation distance, the capillary force corresponding to $r = 1$ for a zero contact angle is more than four times bigger than the same radii ratio but a contact angle of forty.

6 Concluding remarks

By extending the toroidal approximation to non-perfectly wettable particles, the current model covers a wide range of soil mineral grains and liquids. Cases such as perfectly wettable granular assemblies and equal size particles are also recovered as special cases. The numerical approach developed in the present paper can be easily implemented and used to generate solutions for various particle-pair and liquid bridge configurations. The numerical procedure has been built on the special case of perfectly wettable particles for which a robust secant method has been proposed by Harireche et al. [11]. Such a special case is used to start an iterative process where the contact angle is divided into small increments within which Newton-Raphson typical iterations are performed until convergence is achieved. The current model has been validated against the experimental data provided by Rabinovich et al. [12]. The case where the contact angle with each particle is different has not been taken into consideration in the present paper. However, as can be seen from conditions (9) and (10), different values of the angle θ would need to be considered in these two equations and appropriately reflected in the expressions of functions f_3 and f_4 and in the components J_{3a} and J_{4a} $(a=1,\ldots,5)$ of the Jacobian matrix.

Disclosures

This study is not supported by any financial support or funding.

References

[1] Haines, W. B. (1925). Studies in the physical properties of soils: II. A note on the cohesion developed by capillary forces in an ideal soil. J. Agric. Sci. **15**, 529-535, doi: 10.1017/S0021859600082460.

[2] Haines, W. B. (1927). Studies in the physical properties of soils: IV. A further contribution to the theory of capillary phenomena in soil. J. Agric. Sci. **17**, 264-290, doi: 10.1017/S0021859600018499.

[3] Fisher, R.A. (1926). On the capillary forces in an ideal soil. J. Agric. Sci. **16**, 492–505, doi: 10.1017/S0021859600007838.

[4] Fisher, R. A. (1928). Further note on the capillary forces in an ideal soil. J. Agric. Sci. **18**, 406–410, doi: 10.1017/S0021859600019432.

[5] Carman, P. C. (1953). Properties of capillary-held liquids. J. Phys. Chem. **57** (1), 56-64, doi: 10.1021/j150502a012.

[6] Rose, W. J. (1958). Volumes and surface areas of pendular rings. J. app. phys. **29**, 687-691, doi: 10.1063/1.1723251.

[7] Mason, G. & Clark, W. C. (1965). Liquid bridges between spheres. Chem. Eng. Sci. **20**, 859-866, doi: 10.1016/0009-2509(65)80082-3.

[8] Lian, G. P., Thornton, C. & Adams, M. J. (1993). A theoretical study of the liquid bridge forces between two rigid spherical bodies. J. Colloid Interface Sci. **161**, 138–147, doi: 10.1006/jcis.1993.1452.

[9] Willet, C. D., Adams, M.J., Johnson, S. A. & Seville, J. P. K. (2000). Capillary bridges between two spherical bodies. Langmuir **16**, 9396-9405, doi: 10.1021/la000657y.

[10] Schwarze, R., Gladkyy, A., Uhlig, F. & Luding, S. (2013). Rheology of weakly wetted granular materials: a comparison of experimental and numerical data. Granular Matter 15, 455-465, doi: 10.1007/s10035-013-0430-z

[11] Harireche, O., Faramarzi, A. & Alani, A. M. (2013). A toroidal approximation of capillary forces in polydisperse granular assemblies. Granular Matter 15, 573-581, doi: 10.1007/s10035-013-0425-9.

[12] Rabinovich, Y. I., Esayanur M. S. & Moudgil, B. M. (2005). Capillary forces between two spheres with a fixed volume liquid bridge: Theory and experiment. Langmuir **21**, 10992-10997, doi: 10.1021/la0517639.

[13] Willet, C.D., Adams, M.J., Johnson, S.A. & Seville, J.P.K. (2003). Effects of wetting hysteresis on pendular liquid bridges between rigid spheres. Powder Technol. **130**, 63-69, doi: 10.1016/S0032-5910(02)00235-8

Appendix 1

Expressions of functions f_a, $a=1,...,5$, involved in equations 7-10 and 14.

$$f_1(\boldsymbol{X}) = (x_A-\xi)^2+(y_A-\eta)^2-\rho^2$$

$$f_2(\boldsymbol{X}) = (x_B-\xi)^2+(y_B-\eta)^2-\rho^2$$

$$f_3(\boldsymbol{X}) = (s\xi-c\eta)x_A+(c\xi+s\eta)y_A-s$$

$$f_4(\boldsymbol{X}) = (sL+s\xi+c\eta)x_B+(cL-c\xi+s\eta)y_B-L(s\xi+c\eta)-s$$

$$f_5(\boldsymbol{X}) = \pi\left[F_v(x_B)-F_v(x_A)\right]-V_A^*-V_B^*-V_w^*$$

In the expressions above, $F_v(x)$, $V_I^*, I=A,B$ and V_w^* are defined by (15), (12) and (2), respectively. The parameters c and s correspond to $\cos(\theta)$ and $\sin(\theta)$, respectively.

Appendix 2

Expression of the components of the Jacobian matrix defined by equation 18.

$$J_{11}=2\frac{x_A}{y_A}\eta-2\xi;\ J_{12}=0;\ J_{13}=2(\xi-x_A);\ J_{14}=2(\eta-y_A);\ J_{15}=-2\rho;$$

$$J_{21}=0;\ J_{22}=-2\eta\left(\frac{L-x_B}{y_B}\right)-2\xi+2L;\ J_{23}=2(\xi-x_B);\ J_{24}=2(\eta-y_B);$$

$$J_{25}=-2\rho;$$

$$J_{31}=(s\xi-c\eta)-(c\xi+s\eta)\frac{x_A}{y_A};\ J_{32}=0;\ J_{33}=sx_A+cy_A;\ J_{34}=-cx_A+sy_A;$$

$$J_{35}=0;$$

$$J_{41}=0;\ J_{42}=(cL-c\xi+s\eta)\left(\frac{L-x_B}{y_B}\right)+(sL+s\xi+c\eta);\ J_{43}=sx_B-cy_B-Ls;$$

$$J_{44}=cx_B+sy_B-Lc;\ J_{45}=0;$$

$$J_{51}=0;\ J_{52}=0;\ J_{53}=\pi(y_B-y_A)(y_B+y_A-4\eta);$$

$$J_{54}=\pi\left[x_B(\eta+y_B)-x_A(\eta+y_A)-\xi(y_B-y_A)\right]+\pi\rho^2\left[\arctan\left(\frac{x_B-\xi}{y_B-\eta}\right)-\arctan\left(\frac{x_A-\xi}{y_A-\eta}\right)\right]$$

$$J_{55}=2\pi\rho\left[x_B-x_A\right]+2\pi\rho\eta\left[\arctan\left(\frac{x_B-\xi}{y_B-\eta}\right)-\arctan\left(\frac{x_A-\xi}{y_A-\eta}\right)\right].$$

Appendix 3

Algorithm for the numerical procedure to solve equations 7-10 and 14.

(1) Obtain $\boldsymbol{X}^{(1)}$ using the secant procedure proposed in Harireche et al. [11] and set $\boldsymbol{X}^{(0)} = \boldsymbol{X}^{(1)}$

(2) Set increment counter to zero: $inc = 0$

(3) Perform a new increment: $inc \leftarrow inc + 1$

(4) Set iteration counter to zero: $i = 0$

(5) Perform a new iteration: $i \leftarrow i + 1$

(6) Obtain $\Delta \boldsymbol{X}$ by solving: $\sum_{b=1}^{5} J_{ab}(\boldsymbol{X}^{(i-1)})\Delta X_b = f_a(\boldsymbol{X}^{(i-1)})$, $a = 1,...,5$

(7) Obtain $f_a(\boldsymbol{X}^{(i)}) = f_a(\boldsymbol{X}^{(i-1)} + \Delta \boldsymbol{X})$, $a = 1,...,5$

(8) Check convergence: $\|\boldsymbol{F}\| < Tol$; where $\boldsymbol{F}^T = (f_1(\boldsymbol{X}^{(i)}),..., f_5(\boldsymbol{X}^{(i)}))$ and *Tol* is typically 10^{-6}.

(9) If (convergence) Then set $\boldsymbol{X}^{(0)} = \boldsymbol{X}^{(i)}$ and Go to (3)

Else Goto (5)

(10) END

Figure captions:

Figure 1. Normalised geometry of a non-perfectly wettable particle-pair and liquid bridge

Figure 2. Liquid bridge: Normalised water volume and spherical caps.

Figure 3. Model validation against the experiments and analytical expression reported by Rabinovich et al. (2005) for a contact angle, θ = 10°.

Experiment (1): R_A=35μm, V_w=2×10^8 nm^3,

Experiment (2): R_A=32.5μm, V_w=12×10^8 nm^3,

Experiment (3): R_A=27.5μm, V_w=36×10^8 nm^3.

Figure 4. Effect of various contact angles on inter-particle capillary force (V_w=1.32×10^{-2} mm^3, $\sigma = 2.06 \times 10^{-5}$ N/mm, R_A = 2.381 mm and R_B = 1.588 mm)

Figure 5. Scaled capillary force as a function of the scaled separation distance for values of the contact angle, θ = 0° and θ = 40° and scaled liquid volumes, V^*_w = 0.0001 and V^*_w = 0.001 ($\sigma = 2.06 \times 10^{-5}$ N/mm, R_A = 2.381 mm and R_B = 1.588 mm).

Figure 6. Scaled capillary force as a function of the scaled separation distance for values of the contact angle, θ = 0° and θ = 40° and ratios of particle radii, r = 1/2 , r = 2/3 and r = 1 (V_w=1.32×10^{-2} mm^3, $\sigma = 2.06 \times 10^{-5}$ N/mm).

Figures

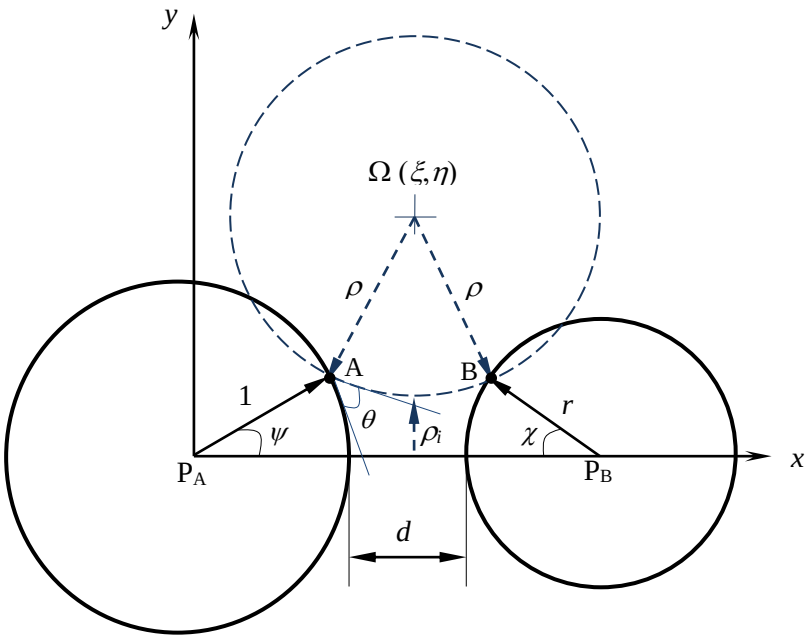

Figure 1

(Created with Microsoft Word)

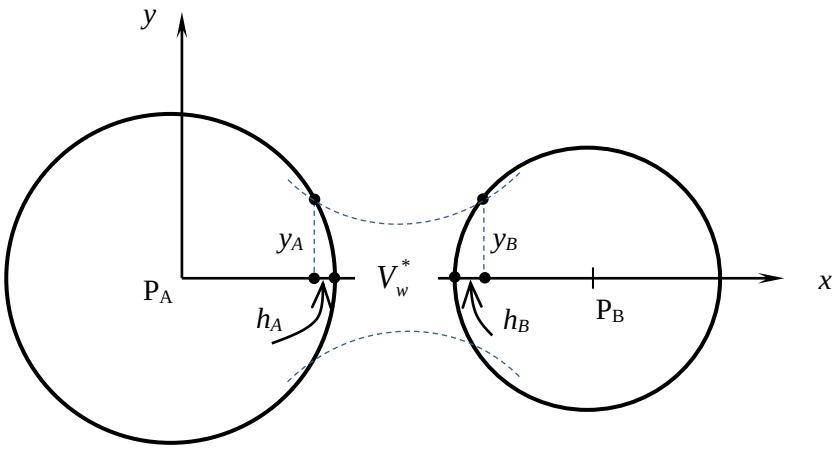

Figure 2

(Created with Microsoft Word)

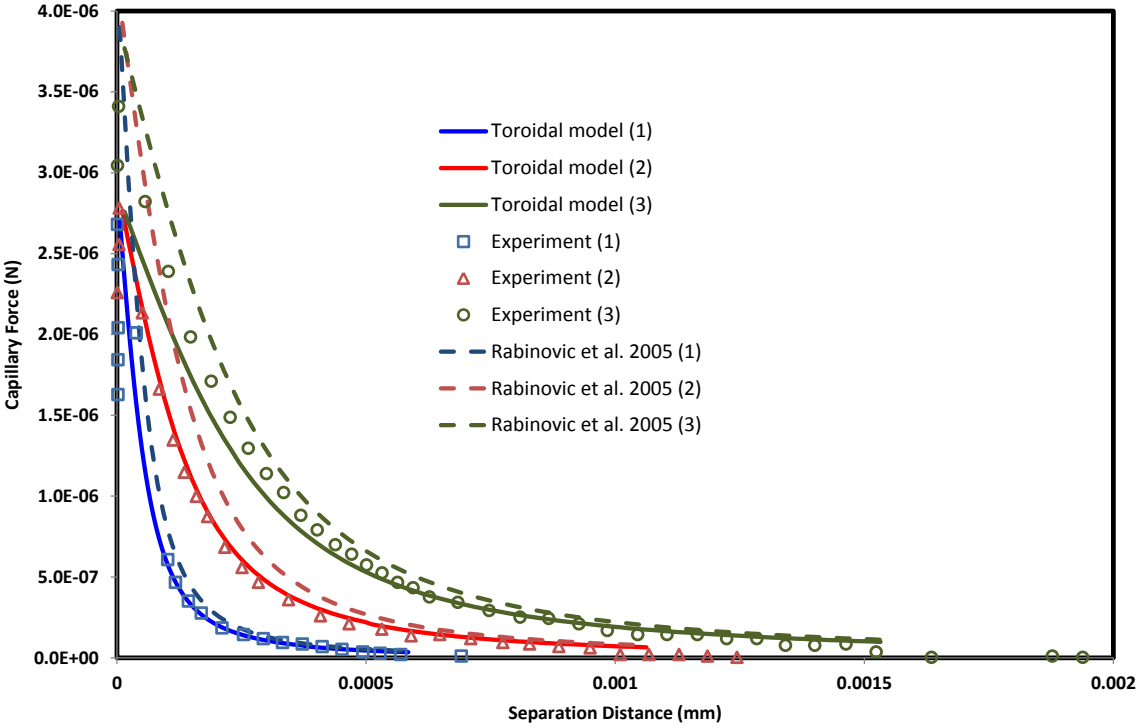

Figure 3

(Created with Microsoft Excel)

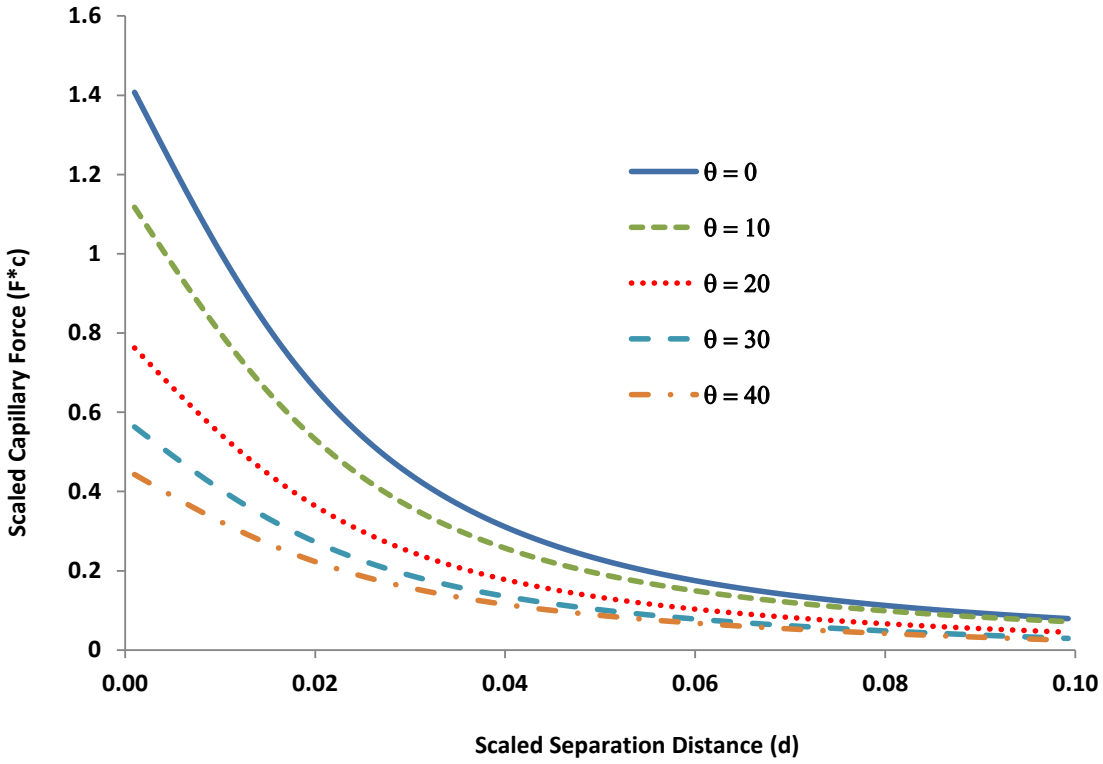
1.6
1.4
1.2
1
0.8
0.6
0.4
0.2
0
Scaled Capillary Force (F*c)
0.00
0.02
0.04
0.06
0.08
0.10
Scaled Separation Distance (d)
θ = 0
θ = 10
θ = 20
θ = 30
θ = 40

Figure 4

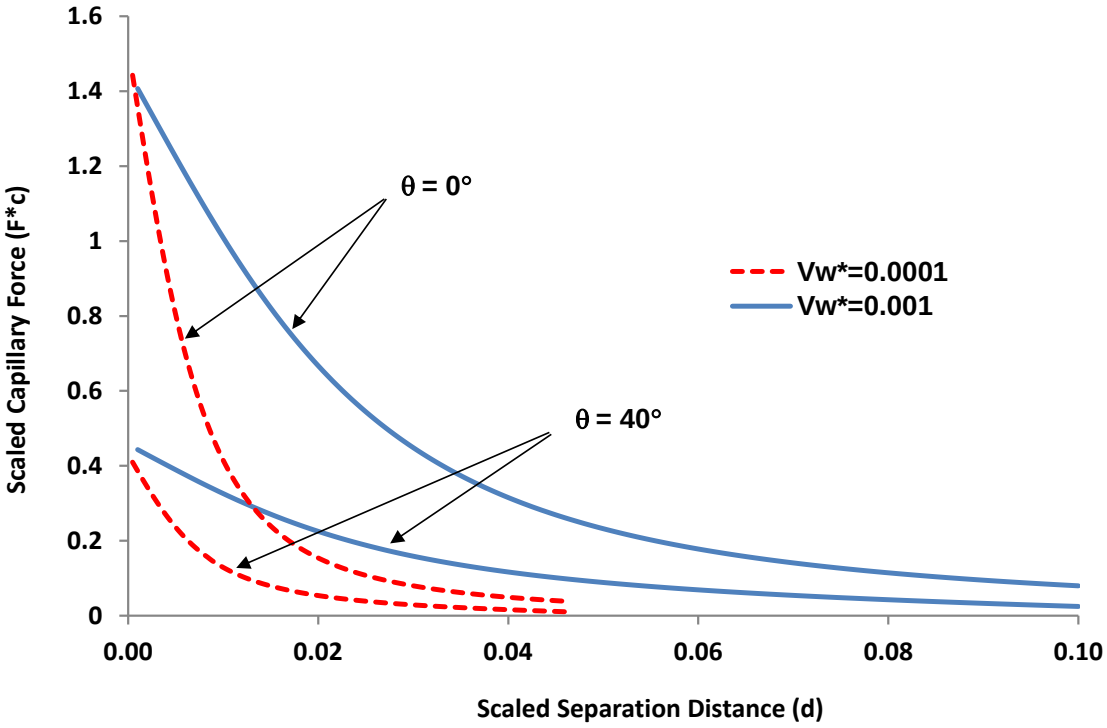
1.6
1.4
1.2
1
0.8
0.6
0.4
0.2
0
0.00
0.02
0.04
0.06
0.08
0.10
Scaled Capillary Force (F*c)
Scaled Separation Distance (d)
θ = 0°
θ = 40°
Vw*=0.0001
Vw*=0.001

Figure 5

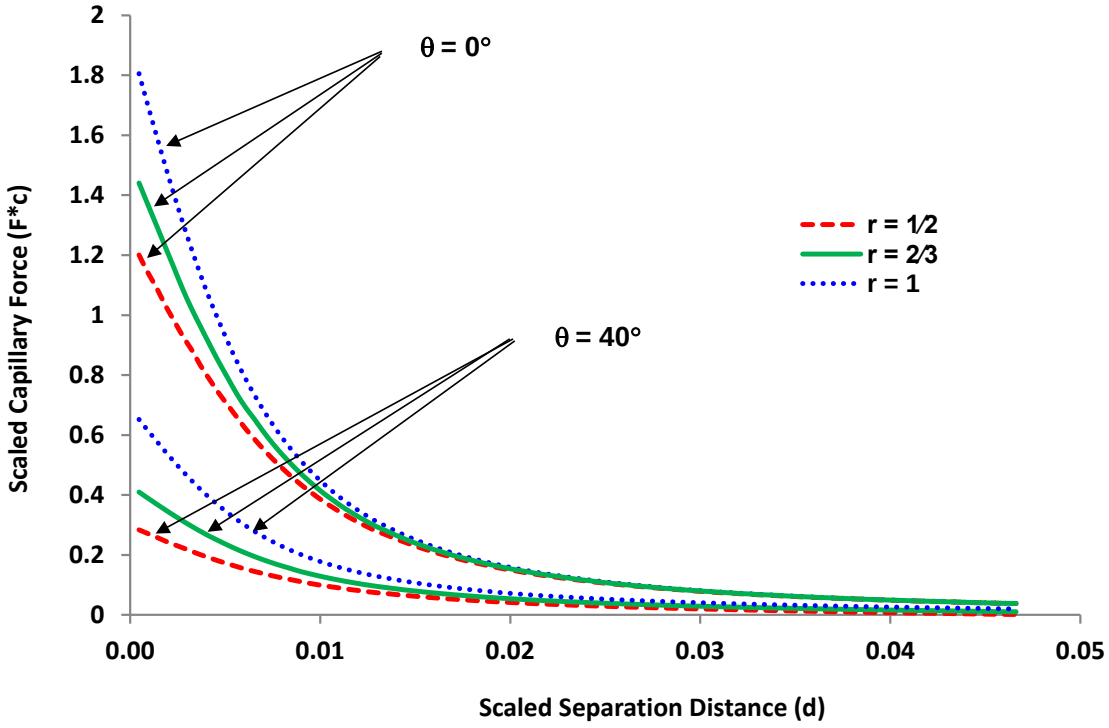
Scaled Capillary Force (F*c)
Scaled Separation Distance (d)
θ = 0°
θ = 40°
r = 1/2
r = 2/3
r = 1
2
1.8
1.6
1.4
1.2
1
0.8
0.6
0.4
0.2
0
0.00
0.01
0.02
0.03
0.04
0.05

Figure 6